Coastal Engineering 67 (2012) 67–79

Contents lists available at SciVerse ScienceDirect

Coastal Engineering

journal homepage: www.elsevier.com/locate/coastaleng

Spectral wave modeling in fringing reef environments

Jean-François Filipot *, Kwok Fai Cheung

Department of Ocean and Resources Engineering, University of Hawaii at Manoa, Honolulu, HI 96822, USA

ARTICLE INFO

Article history:
Received 26 August 2011
Received in revised form 5 April 2012
Accepted 10 April 2012
Available online 22 May 2012

Keywords:
Bottom friction
Fringing reefs
Phase-averaged model
Spectral model
SWAN
Wave breaking

ABSTRACT

This study examines the implementation and validity of phase-averaged spectral models in describing wave transformation over fringing reefs. The wave breaking mechanism over the abrupt reef crest, dissipation due to bottom friction, and nonlinear energy transfer over the reef flat set the problem apart from general applications in non-tropical settings. The Simulating Wave Nearshore (SWAN) model, which is widely used in coastal engineering applications, has embedded parameterizations of these surf-zone processes for examination. In addition, we extend the model to include a recently implemented bottom-friction source term for tropical reefs. Comparisons of model predictions with laboratory and field observations over fringing reefs identify promising wave-breaking and bottom-friction parameterizations for calibration. The calibrated parameterizations enable SWAN to reproduce the observed wave height and setup and extend the applicability of spectral models to fringing reef environments. SWAN, however, lacks the parameterization to describe the nonlinear energy transfer toward the infra-gravity band that was observed in the laboratory and field studies.

1. Introduction

Spectral wave models are widely used around the world for numerous applications from operational wave predictions at global and regional scales to site-specific coastal engineering applications. These models provide a phase-averaged description of the generation and propagation of ocean waves subject to wind forcing. Let f denote the frequency and θ the wave direction. The evolution of the wave energy density spectrum $E(f,\theta)$ in time and space is defined by the energy balance equation

$$\frac{dE(f,\theta)}{dt} = S \tag{1}$$

where d/dt denotes material derivative and S the source term (Gelci et al., 1957). In third generation spectral wave models, the spectrum can describe multi-modal sea states and the source term contains parameterizations of the physical processes that include energy input by winds, nonlinear energy transfer among frequency components, and dissipation through wave breaking and bottom friction (e.g., Tolman, 2008; Komen et al., 1994; Booij et al., 1999; Zijlema, 2010). These models owe their success to their low computational costs and proven accuracy for typical ocean conditions due in part to the extensive and continuing efforts on parameterization of the physics involved (e.g., Ardhuin et al., 2010). The early parameterizations have been mostly designed for the open ocean, but efforts have been made to extend their capabilities and implementations to shallow water (Eldeberky, 1996; Ris et al., 1999; Filipot and Ardhuin, in press). Although the accuracy of these parameterizations has been extensively examined for continental beach environments, very little is known on their ability to model wave transformation over fringing reefs.

Commonly found in the tropics and subtropics, fringing reefs are characterized by a steep slope with an abrupt transition at the reef crest to a shallow platform attached to the shoreline. Intense wave breaking typically occurs around the reef crest enhancing the oxygen content and circulation that support the coral ecosystem (Abelson et al., 1993). Wave breaking at fringing reefs protects the coastline from severe wave conditions, but increases the water level due to wave setup (e.g. Vetter et al., 2010). Over the flat, the bottom friction associated with the reef formation and corals may dissipate as much energy as wave breaking (Lugo-Fernández et al., 1998; Lowe et al., 2005). Although the nonlinear triad interactions of the frequency components are energy conservative, they cause dramatic alteration of the spectral shape across the reef. Energy is transferred from the spectral peak to the super-harmonics during the shoaling phase (Eldeberky, 1996), making the wave crest sharper and the trough flatter, and then toward the infra-gravity band in the surf zone (Sheremet et al., 2011). Seiching occurs if the natural period of the reef flat matches the infra-gravity band (Nwogu and Demirbilek, 2010; Roeber et al., 2010a, 2010b; Péquignet et al., 2011). These processes, which have important implications for coastal protection as well as for the fragile coral ecosystem, have drawn a growing interest in the community.

Because of the low computational cost, the capability to account for wind effects, and ready coupling with a circulation model for storm surge computations, researchers and engineers have applied spectral wave models to tropical and subtropical coastal regions without

* Corresponding author at: Service Hydrographique et Océanographique de la Marine, Brest, France. Tel.: +33 298 149 936.
E-mail addresses: filipot@shom.fr (J-F. Filipot), cheung@hawaii.edu (KF. Cheung).

0378-3839/$ – see front matter © 2012 Elsevier B.V. All rights reserved.
doi:10.1016/j.coastaleng.2012.04.005

knowing the full impact of their limitations. The motivation of this study is to assess the validity of spectral wave models for application in fringing reef environments. We examine the parameterizations for wave breaking and bottom-friction in the commonly-used Simulating Wave Nearshore (SWAN) model (Booij et al., 1999; Ris et al., 1999). In addition, we implement the bottom friction parameterization of Lowe et al. (2005) for a barrier reef in SWAN. A comparison with the laboratory data from Demirbilek et al. (2007) for wave transformation and setup over a smooth reef configuration provides an initial assessment of the wave breaking parameterizations and identification of a promising scheme for calibration. A general assessment of the bottom-friction parameterizations in SWAN is made with 10 days of observational data over a fringing reef on North Shore, Oahu, Hawaii. The dataset allows calibration of the parameterization of Lowe et al. (2005) for the fringing reef at the site. In both case studies, the ability of SWAN in reproducing both the total energy and the spectral shape is examined and the advantages and limitations of spectral wave modeling are discussed.

2. Modeling of coastal processes

The governing Eq. (1) for phase-averaged spectral models already accounts for wave shoaling and refraction in the evolution of the energy density spectrum over time and space. Other coastal processes such as depth-induced wave breaking, dissipation due to bottom friction, and triad nonlinear energy transfer among frequency components are included in the source term through parameterization of the physical processes. This section provides a brief review of these parameterizations in SWAN, the formulation of Lowe et al. (2005) for bottom friction in reef environments, and the computation of wave setup.

2.1. Depth-induced wave breaking

The physical processes of wave breaking are complex and its spectral signature is still an active field of research (e.g., Vink, 2001; Filipot et al., 2010). The parameterization of the processes includes the wave breaking probability and the subsequent dissipation rate. In shallow water, the breaker index limits the wave height H to a fraction of the water depth d as

$$\gamma = \frac{H}{d} \tag{2}$$

Longuet-Higgins (1974) derived $\gamma = 0.78$ from solitary wave theory. For irregular waves on a sloping bottom, the breaker index varies over a wide range. For instance, Raubenheimer et al. (1996) observed values ranging from 0.3 to 1.2 based on the significant wave height H_s. Several hypotheses were advanced to explain the variability of the breaker index in terms of the offshore wave steepness (Battjes and Stive, 1985), the bottom slope (Raubenheimer et al., 1996; Nelson, 1987), the water depth parameter kd, where k is the wave number (Ruessink et al., 2003), and the phase angle of the complex bi-spectrum (van der Westhuysen, 2010). The dissipation rate is typically formulated by approximation of the broken waves as bores with heights inferred from probability density functions based on the Rayleigh distribution (Goda, 1975; Battjes and Janssen, 1978; Thornton and Guza, 1983).

SWAN includes five parameterizations to describe depth-induced wave breaking processes. The formulation by Battjes and Janssen (1978), hereafter BJ78, provides the framework for three of the parameterizations, in which the total dissipation rate is given by

$$D_{tot} = \frac{1}{4} B Q_B \bar{f} H_m^2 \tag{3}$$

where B is a constant controlling the level of energy dissipation, $\bar{f}$ is the mean frequency, H_m is the maximum wave height in terms of the breaker index (2), and Q_B is the breaking probability of the random sea state. The breaking probability Q_B can be estimated by means of

$$\frac{1-Q_B}{-\ln Q_B} = \left(\frac{H_{rms}}{H_m}\right)^2 \tag{4}$$

where H_{rms} is the root-mean-square wave height. The breaker index is the key parameter in the energy dissipation formulation. Battjes and Janssen (1978) provided $\gamma = 0.73$ from a wide range of wave breaking observations on beaches. From laboratory and field data, Nelson (1987, 1994, 1994), hereafter NE87, introduced a dependence of the breaker index on the bottom slope α as

$$\gamma = 0.55 + 0.88 exp[-0.012 cot(\alpha)] \tag{5}$$

in which γ varies from 0.55 for horizontal bottoms to 1.3 for very steep slopes. From analysis of two datasets gathered in barred beach environments, Ruessink et al. (2003), hereafter RU03, reported a dependence of the breaker index on the water depth parameter as

$$\gamma = 0.76kd + 0.29 \tag{6}$$

In BJ78, NE87 and RU03, the breaker index defines a single maximum wave height after the onset of breaking and thus also controls the dissipation rate in the surf zone.

Thornton and Guza (1983), hereafter TG83, parameterized the dissipation rate with a distribution of breaking wave heights in contrast to the approaches based on BJ78. The total dissipation rate in the random wave field is given by

$$D_{tot} = -\frac{B^3 \bar{f}}{4} \frac{\bar{f}}{d} \int_0^\infty H^3 P(H) W(H) dH \tag{7}$$

in which P is the Rayleigh distribution and W is a weight function given by

$$W(H) = \left(\frac{H_{rms}}{\gamma d}\right)^2 \tag{8}$$

where a breaker index of $\gamma = 0.42$ is predefined in the parameterization. Van der Westhuysen (2010), hereafter WE10, assumes a constant distribution of the weight function and parameterizes the biphase, which accounts for wave asymmetry and hence the nonlinearity and breaking susceptibility. The resulting dissipation rate is

$$D_{tot} = -\frac{3\sqrt{\pi}}{16} \frac{B^3 \bar{f}}{d} \left(\frac{\beta}{\beta_{ref}}\right)^2 H_{rms}^3 \tag{9}$$

in which the biphase is expressed in terms of the Ursell number Ur as

$$\beta = \frac{-\pi}{2} + \frac{-\pi}{2} \tanh\left(\frac{0.2}{U_r}\right) \tag{10}$$

and $\beta_{ref} = -4\pi/9$. Note that, in relating the breaking probability to wave nonlinearity, this approach shares some similarities with the work of Filipot et al. (2010).

The breaking probability and dissipation rate produce reasonable results for continental shelf beaches with gentle slopes. In SWAN, a default value of $B = 1$ is typically used. The total dissipation is distributed over the frequency range and direction bins in proportion to the spectral density. The source term for depth-induced breaking dissipation is given by

$$S_{bk}(f,\theta) = D_{tot} \frac{E(f,\theta)}{E_{tot}} \tag{11}$$

where D_{tot} is the dissipation rate from Eqs. (3), (7) or (9) depending on the parameterization and E_{tot} is the total spectral energy from integration of $E(f,\theta)$. This approach, which does not alter the spectral shape during the wave breaking process, is consistent with the findings of Eldeberky and Battjes (1996) from flume experiments involving single-peaked spectra.

2.2. Bottom friction

When the water depth becomes less than one half of the wavelength, the wave orbital motions extend to the bottom resulting in energy dissipation via various linear or nonlinear processes. Shemdin et al. (1978) identified and examined four dissipation processes: wave orbital velocity friction on the bed, percolation of the water particles through the bottom substrate, wave-induced motion of a soft muddy bottom, and scattering of surface waves by bottom irregularities. Friction dominates in sandy and hard substrate conditions commonly found along the world's coastlines. The shear stress and the dissipation rate are typically parameterized in terms of a drag law or an eddy viscosity model (Mirfenderesk and Young, 2003). In spectral wave models, the dissipation source term for bottom friction can be expressed as

$$S_{bf}(f,\theta) = -C_b \frac{(2\pi f)^2}{g^2 \sinh^2 kd} E(f,\theta) \tag{12}$$

where g is acceleration due to gravity and C_b is a bottom friction coefficient derived from parameterization of the physical processes (Bertotti and Cavaleri, 1994).

SWAN includes three bottom-friction parameterizations based on the empirical JONSWAP model of Hasselmann et al. (1973), the drag law model of Collins (1972), and the eddy viscosity model of Madsen (1988). The empirical JONSWAP model assumes a constant C_b of 0.038 $m^2\,s^{-3}$ from observations of swell energy decay in the North Sea even though the observed value varies over two orders of magnitude during the field study. The drag law model, which is primarily a simplification of Hasselmann and Collins (1968) for regular waves, can be written as

$$C_b = C_f g U_{rms} \tag{13}$$

where $C_f = 0.015$ and U_{rms} is the root-mean-square wave orbital velocity at the bottom. Madsen (1988) proposed a formulation based on the eddy viscosity model yielding:

$$C_b = f_w \frac{g}{\sqrt{2}} U_{rms} \tag{14}$$

in which the friction coefficient f_w is given by Jonsson (1967) as

$$\frac{1}{4\sqrt{f_w}} + log_{10}\left(\frac{1}{4\sqrt{f_w}}\right) = -0.08 + log_{10}\left(\frac{a_{b,r}}{K_w}\right) \tag{15}$$

where $a_{b,r}$ is a representative bottom orbital amplitude and K_w denotes the hydraulic roughness scale. SWAN does not include the effect of a mean current on the bottom friction (Booij et al., 1999). According to Tolman (1992), the impact of the current is negligible compared to the error in the estimation of a correct hydraulic roughness scale.

In addition, we implemented the bottom-friction parameterization of Lowe et al. (2005), hereafter LW05, into SWAN. Their work is based on Madsen (1994), in which the bottom-friction coefficient is expressed in terms of a frequency-dependent dissipation factor $f_e(\sigma)$ as

$$C_b = \frac{g U_{rms}}{4} f_e(\sigma) \tag{16}$$

The energy dissipation factor is in turn given by

$$f_e(\sigma) = \sqrt{f_w(\sigma_r)}\sqrt{f_w(\sigma)}\cos\varphi(\sigma) \tag{17}$$

in which the wave friction factor, the phase relation between shear stress and velocity, and the representative radian-frequency are given by

$$f_w(\sigma) = \exp\left[a_1\left(\frac{U_{rms}}{\sigma K_w}\right)^{a_2} + a_3\right] \tag{18}$$

$$\varphi(\sigma) = 33 - 6.0 log_{10}\left(\frac{U_{rms}}{K_w \sigma}\right) \tag{19}$$

$$\sigma_r = \int_0^\infty \sigma u_b^2(\sigma) d\sigma \Big/ \int_0^\infty u_b^2(\sigma) d\sigma \tag{20}$$

This formulation involves a number of free parameters for calibration. LW05 used the empirical coefficients $a_1 = 5.5$, $a_2 = -0.2$, and $a_3 = -6.3$ from Nielsen (1992) to facilitate calculation of the hydraulic roughness scale from measurements. They determined an optimal value of $K_w = 0.16$ m through comparison of an energy flux model with observed dissipation rates, in the absence of breaking waves, along a cross-shore transect on a barrier reef at Kaneohe, Hawaii. It is remarkable that physical measurements with a profiler at 14 locations on the reef flat revealed very similar values of $K_w = 0.14 \pm 0.03$ m, suggesting nearly homogenous surface roughness over the study area and the consistence of the method itself.

2.3. Triad interactions

The triad interactions dominate the nonlinear energy transfer among frequency components in coastal waters with $kd < 1$. During shoaling, wave energy cascades down from the spectral peak to the super-harmonics resulting in wave profiles with steeper crests and flatter troughs. The crest loses its vertical symmetry and continues to steepen prior to wave breaking. Eldeberky (1996) provided a description of these effects resulting from the triad interactions through an energy density formulation of the Boussinesq model of Madsen and Sørensen (1993). Although the formulation only includes self interactions of collinear waves, it provides a reasonable description of the energy transfer to the super-harmonics for general application.

The parameterization adopted in SWAN, known as the lumped triad approximation (LTA) in Eldeberky (1996), relies on an empirical expression for the biphase, derived from the laboratory experiments of Battjes and Beji (1992) and Arcilla et al. (1994). The source term for the triad interactions is written as

$$S_{nl3}(f,\theta) = S_{nl3}^{-}(f,\theta) + S_{nl3}^{+}(f,\theta) \tag{21}$$

in which

$$S_{nl3}^{+}(f,\theta) = \max\left\{0, \alpha_{EB} 2\pi c c_g J^2 \left|\sin(\beta)\right| \left[E^2(f/2,\theta) - 2E(f/2,\theta)E(f,\theta)\right]\right\} \tag{22}$$

$$S_{nl3}^{-}(f,\theta) = -2S_{nl3}^{+}(2f,\theta) \tag{23}$$

where the biphase β is given by the parameterization (10), c and c_g are the celerity and group velocity, respectively, α_{EB} is a predefined constant, and J is a coupling coefficient of the triad interactions derived from the energy density formulation of Madsen and Sørensen (1993).

2.4. Wave setup

The depth-induced breaking and bottom-friction parameterizations play an important role in defining the coastal wave height, which in turn modifies the water level through the radiation stresses. The water-level increase along the shore, known as wave setup, is important to flood hazard assessment and beach safety. SWAN may provide the radiation stresses to a circulation model for computation of wave-induced currents and water-level variations in the surf zone. This is commonly

done in modeling of storm surge due to hurricane landfalls (e.g., Cheung et al., 2007; Dietrich et al., 2010). Alternatively, SWAN may directly provide an estimate of the wave setup by assuming stationary wave conditions.

Let (x, y) define the Cartesian coordinate system in the horizontal plane. In one dimension, SWAN solves the momentum balance equation, in which the hydrostatic pressure gradient balances the phase-averaged force induced by the waves. The variation of the mean surface elevation $\bar{\eta}$ is expressed in terms of the radiation stress S_{xx} as

$$\frac{d\bar{\eta}}{dx} = -\frac{1}{\rho g(d+\bar{\eta})}\frac{dS_{xx}}{dx} \tag{24}$$

For two-dimensional cases, SWAN estimates the variation of the mean surface elevation from the Poisson equation

$$\frac{\partial F_x}{\partial x} + \frac{\partial F_y}{\partial y} + \frac{\partial}{\partial x}\left[\rho g(d+\bar{\eta})\frac{\partial \bar{\eta}}{\partial x}\right] + \frac{\partial}{\partial y}\left[\rho g(d+\bar{\eta})\frac{\partial \bar{\eta}}{\partial y}\right] = 0 \tag{25}$$

in which

$$F_x = -\frac{\partial S_{xx}}{\partial x} - \frac{\partial S_{xy}}{\partial y} \tag{26}$$

$$F_y = -\frac{\partial S_{yy}}{\partial y} - \frac{\partial S_{yx}}{\partial x} \tag{27}$$

are the rotation-free part of the wave-induced forces determined from the radiation stresses in the x-y plane (Dingemans, 1987). The reader may refer to Holthuijsen (2007) for the full expressions of the radiation stresses and for more details on the wave setup calculations in SWAN.

3. Comparison with wave flume data

Demirbilek et al. (2007) reported a flume experiment on wave transformation over a fringing reef that allows comparison and calibration of the parameterizations for wave breaking dissipation. The flume, which is 35 m long, 0.7 m wide, and 1.6 m high, features a 1:64 scaled model of a reef typical of the southeast shore of Guam. Fig. 1 shows the locations of 9 wave gages and the profile of the model that includes a composite slope for the reef face, a reef flat, and a beach. The measurements at G4 are not used here as they were found to be inaccurate. The toe of the reef is located at 15.5 m from a plunger-type wave maker, which generates irregular sea states based on the JONSWAP spectrum with random phases. As the reef model was built of polyvinyl chloride (PVC), bottom friction is negligible for the smooth and impervious material. We may assume, at least in the vicinity of the reef crest, that depth-induced breaking is the only dissipation mechanism. Table 1 lists the 19 test cases, which cover the input significant wave height $H_s = 3.2$–8.5 cm, peak period $T_p = 1$–2.5 s, and water depth $h_r = 1.6$–5.1 cm over the reef flat. These correspond to offshore waves with heights and periods up to 5.4 m and 20 s respectively and at least 1 m of water over the reef flat in the prototype.

The five parameterizations for depth-induced wave breaking in SWAN are examined through the 19 test cases. The computational domain extends from G1 to the end of the flume at 1 cm resolution. The incident wave spectrum recorded at G1 provides the boundary condition for the calculation with 42 frequency bins from 0.05 to 3 Hz. SWAN is run in the stationary and one-dimensional Cartesian modes with the triad source term and the setup calculation activated. We first focus on the ability of the five parameterizations in their default settings to predict the significant wave height across the reef. Fig. 2 shows the results from 6 cases representative of the incident wave heights, periods, and water levels considered. The incident waves typically break between G5 and G7 and evolve into turbulent

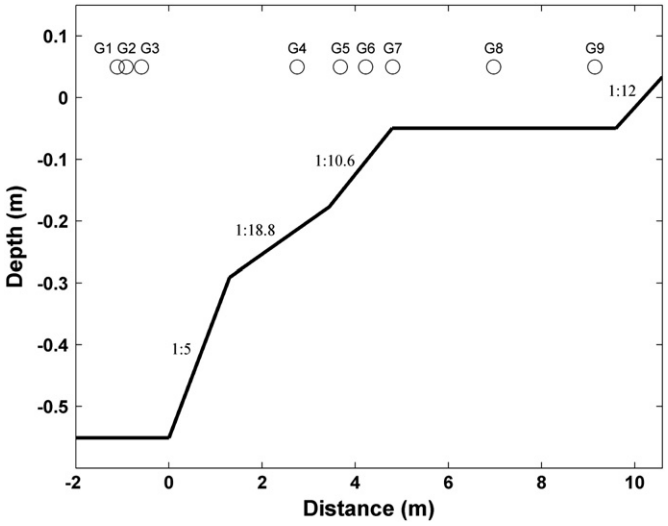

Fig. 1. Schematic and instrument locations for the reef experiment of Demirbilek et al. (2007). The reference elevation at zero corresponds to a water depth of 5.1 cm on the reef flat for illustration. Circles: wave gages.

bores on the reef flat. The model with the various parameterizations performs reasonably well in describing the wave height at the onset of the breaking process and in the surf zone for the low-energy test 20. The discrepancy between the measurements and the computed data increases with the incident wave height. For the energetic wave conditions in tests 19, 48, and 32, all the parameterizations with default settings result in excessive energy dissipation prior to wave breaking leading to underestimation of the wave height at the onset near the reef crest. The model over-predicts the extent of the surf zone resulting in excessive dissipation and underestimation of the energy on the reef flat. The increase of the measured wave height from G8 to G9 in tests 48 and 32 might be attributed to reflection from the beach and formation of partial standing waves.

The overall performance of the five parameterizations in the 19 tests is assessed with four metrics. The Root Mean Square Error (*RMSE*), the Normalized Root Mean Square Error (*NRMSE*), the bias

Table 1
Water depth over the reef flat and input wave conditions for the laboratory tests of Demirbilek et al. (2007).

Test	h_r (cm)	H_s (cm)	T_p (s)
15	5.1	6.2	1.00
20	5.1	6.1	1.25
16	5.1	5.2	1.50
17	5.1	7.8	1.50
21	5.1	8.2	1.75
18	5.1	8.5	2.00
19	5.1	8.3	2.50
26	1.6	5.8	1.00
27	1.6	5.5	1.25
28	1.6	4.7	1.50
29	1.6	7.1	1.50
30	1.6	7.6	1.75
31	1.6	8.5	2.00
32	1.6	7.9	2.50
44	3.1	3.2	1.00
45	3.1	6.1	1.00
46	3.1	5.9	1.25
47	3.1	5.0	1.50
48	3.1	7.5	1.50
57	3.1	7.7	1.75
58	3.1	8.5	2.00
59	3.1	8.2	2.50

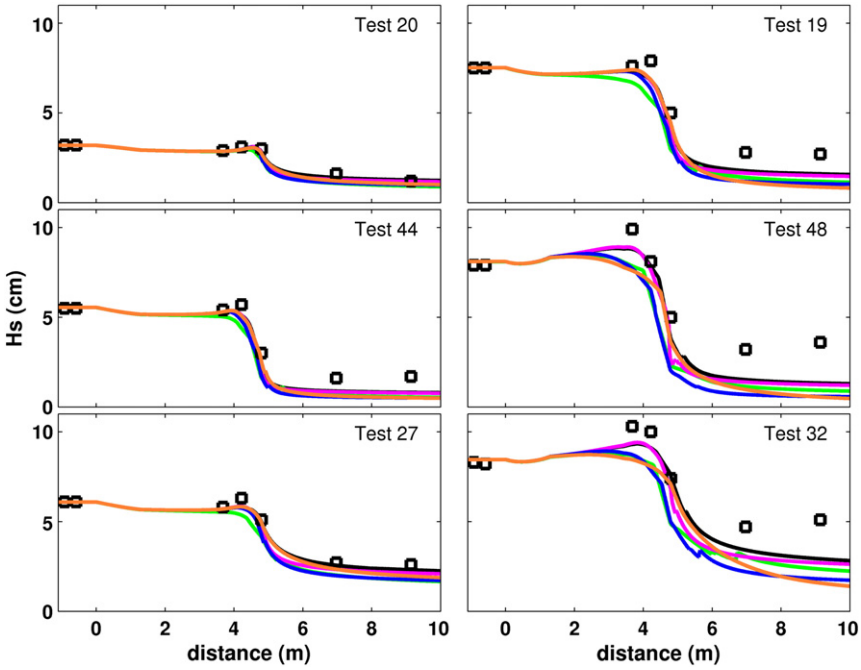

Fig. 2. Comparison of observed and computed significant wave heights for 6 representative test cases. Black squares: measurements; black line: BJ78 with $\gamma = 0.73$ and $B = 1$ (default); green line: TG83; magenta line: NE87; blue line: RU03; orange line: WE10.

(B), and the normalized bias (NB) between the modeled and observed significant wave heights (H_m, H_o) at each gage are defined as

$$RMSE(m) = \sqrt{\frac{\sum_{i=1}^{n}\left(H_{m,i} - H_{o,i}\right)^2}{n}} \tag{28}$$

$$NRMSE(\%) = 100\% \times \sqrt{\frac{\sum_{i=1}^{n}\left(H_{m,i} - H_{o,i}\right)^2}{\sum_{i=1}^{n}\left(H_{o,i}\right)^2}} \tag{29}$$

$$B(m) = \frac{\sum_{i=1}^{n}\left(H_{m,i} - H_{o,i}\right)}{n} \tag{30}$$

$$NB(\%) = 100\% \times \frac{\sum_{i=1}^{n}\left(H_{m,i} - H_{o,i}\right)}{\sum_{i=1}^{n}\left(H_{o,i}\right)} \tag{31}$$

where $n = 19$ denotes the number of tests. Table 2 summarizes the results from the error analysis for the five parameterizations. BJ78 yields the lowest errors overall. This outcome is unexpected as, for instance, NE87 seems to be more suitable because it is a refined version of BJ78 featuring the effect of the bottom slope. The reason is that the breaking index (5) in NE87 is capped at 0.81 in SWAN corresponding to a bottom slope of 0.01 (Booij et al., 1999), which is much smaller compared to that on the reef face in the experiment. However, uncapping the breaker index would lead to a non-physical value of $\gamma = 1.35$ for the reef slope of 0.106 in the experiment. WE10 appears to be a good candidate because the parameterization of the biphase is expected to relate the wave nonlinearity and the onset of wave breaking more precisely. However, WE10 as well as TG83 and RU03 initiate the breaking process earlier than BJ78 resulting in a strong bias of the predictions across the reef.

The results from BJ78, which already have the lowest errors, might be further improved by increasing the breaker index γ. This delays the breaking onset and reduces the width of the surf zone. However, waves tend to break as a plunger over the reef crest and propagate as turbulent bores over the flat (Roeber et al., 2010a, 2010b). The breaking process is more dissipative and the breaking intensity B needs adjustment as well. We conducted a sensitivity analysis by varying γ and B

Table 2
Error metrics for depth-induced wave breaking parameterizations.

Parameterization	Gage	RMSE (cm)	NRMSE (%)	BIAS (cm)	NBIAS (%)
BJ78	G2	0.10	1.43	0.07	1.00
($\gamma = 0.73$, B = 1)	G3	0.16	2.37	0.09	1.43
	G5	0.43	5.95	−0.30	−4.39
	G6	0.63	8.97	−0.57	−8.28
	G7	0.65	13.41	−0.56	−12.00
	G8	0.92	32.67	−0.79	−30.07
	G9	1.24	42.95	−1.03	−38.56
TG83	G2	0.10	1.43	0.07	1.00
	G3	0.16	2.36	0.09	1.41
	G5	0.97	13.41	−0.77	−11.15
	G6	1.46	20.68	−1.36	−19.81
	G7	1.80	37.02	−1.69	−36.40
	G8	1.25	44.56	−1.16	−44.07
	G9	1.62	56.04	−1.44	−54.06
NE87	G2	0.10	1.43	0.07	1.00
	G3	0.16	2.37	0.09	1.43
	G5	0.38	5.30	−0.26	−3.77
	G6	0.64	9.00	−0.57	−8.35
	G7	1.10	22.68	−0.98	−20.98
	G8	1.06	37.80	−0.94	−35.75
	G9	1.34	46.37	−1.13	−42.42
RU03	G2	0.10	1.43	0.07	1.00
	G3	0.16	2.37	0.09	1.42
	G5	0.80	11.02	−0.51	−7.35
	G6	1.20	16.95	−1.05	−15.24
	G7	1.70	35.01	−1.58	−33.92
	G8	1.53	54.49	−1.39	−52.71
	G9	1.80	62.49	−1.58	−59.06
WE10	G2	0.10	1.43	0.07	1.00
	G3	0.16	2.37	0.09	1.43
	G5	0.80	11.14	−0.48	−6.88
	G6	0.88	12.48	−0.78	−11.36
	G7	0.67	13.80	-0.60	−12.98
	G8	1.44	51.32	−1.31	−49.47
	G9	1.92	66.51	−1.67	−62.56

Table 3
Error metrics for the depth-induced wave breaking parameterization BJ78 with $\gamma = 0.94$ and $B = 1.09$.

Gage	RMSE (cm)	NRMSE (%)	BIAS (cm)	NBIAS (%)
G2	0.10	1.44	0.07	1.01
G3	0.16	2.38	0.10	1.45
G5	0.24	3.30	−0.12	−1.85
G6	0.37	5.25	−0.08	−1.12
G7	0.37	7.62	0.06	1.39
G8	0.57	20.17	−0.30	−11.19
G9	0.85	29.62	−0.55	−20.72

from 0.7 to 1.3 at 0.01 increments for each test case. The optimal values of $\gamma = 0.94$ and $B = 1.09$ minimize the average *NRMSE* at G5, G6, G7 and G8 around the reef crest, where intensive wave breaking occurs. This confirms, *a posteriori*, the logic of the optimization. Table 3 shows an appreciable improvement of the error metrics in comparison to the default BJ78 parameterization in SWAN. Fig. 3 shows that the optimal BJ78 parameterization gives better overall agreement with the observed wave height in comparison to the default setting. Most importantly, the present parameterization captures the onset of the breaking process at the reef crest as observed in the experiment. The breaking process and the subsequent wave height attenuation defines the wave setup in the surf zone. Fig. 4 shows the computed and observed wave setup at G8 over the reef flat and Table 4 summarizes the error metrics. The optimal BJ78 parameterization represents an improvement over the default setting to give the best agreement with the observed data. The other parameterizations underestimate the setup comparing to the BJ78 default setting because of the wider predicted surf zones. The optimal values of γ and B provide a convenient setting in BJ78 for practical applications with general wave conditions in fringing reef environments, even though their values as well as other parameterizations can be optimized on a case by case basis (Massel and Gourlay, 2000; Apotsos et al., 2008; Sheremet et al., 2011).

The spectral transformation provides further insights into the wave processes. Fig. 5 compares the observed spectra across the reef with the computed results from the optimal BJ78 parameterization

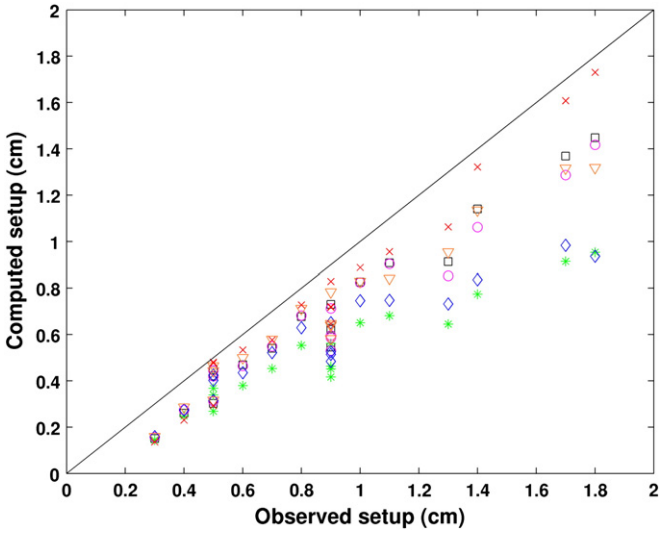

Fig. 4. Scatter plot for wave setup at G8. Red crosses: optimal BJ78 with $\gamma = 0.94$ and $B = 1.09$; Black squares: BJ78 with $\gamma = 0.73$ and $B = 1$ (default); green asterisks: TG83; magenta circles: NE87; blue diamonds: RU03; orange triangles: WE10.

for representative conditions in the experiment. Test 44 with input $H_s = 3.4$ cm and $T_p = 1$ s represents low energy wave conditions with the breaking onset at the reef crest between G6 and G7, while the more energetic test 32 with $H_s = 8.4$ cm and $T_p = 2.5$ s produces breaking waves between G5 and G6, before reaching the reef crest. The wave breaking parameterization captures the energy reduction across the reef in both cases. Nonlinear energy transfer is evident as the waves shoal over the reef slope with development of super and sub-harmonics. The triad source term reproduces the growth of the super-harmonics at twice the peak frequency, but does not describe the sub-harmonics due to the lack of proper parameterization in SWAN. The computed spectrum at G8 shows the same peaks as it does before breaking, while the

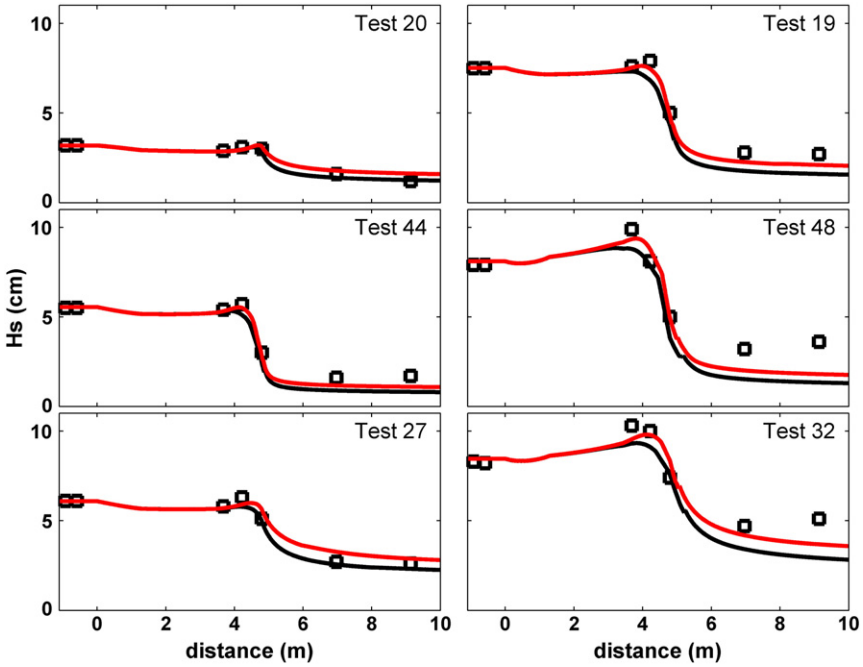

Fig. 3. Comparison of observed and computed significant wave heights for 6 representative test cases. Black squares: measurements, black line: BJ78 with $\gamma = 0.73$ and $B = 1$ (default), red line: optimal BJ78 with $\gamma = 0.94$ and $B = 1.09$.

Table 4
Error metrics of computed wave setup at G8 on the reef flat.

	RMSE (cm)	NRMSE (%)	BIAS (cm)	NBIAS (%)
TG83	0.44	10.57	−0.38	−42.82
NE87	0.26	6.18	−0.23	−25.48
RU03	0.39	9.43	−0.33	−36.34
WE10	0.24	5.70	−0.21	−22.86
BJ78 ($\gamma = 0.73$, B = 1)	0.23	5.56	−0.21	−23.48
BJ78 ($\gamma = 0.94$, B = 1.09)	0.14	3.42	−0.13	−13.99

observed spectrum broadens with a significant part of the energy shifted toward the infra-gravity band. For the same set of laboratory data, Sheremet et al. (2011) managed to reproduce both the sub and super-harmonics with fully nonlinear, triad interaction models.

4. Comparison with field data

With the depth-induced breaking processes calibrated, we focus our attention on dissipation due to bottom friction in natural reef environments. The US Army Corps of Engineers PILOT project provided wave measurements across a fringing reef off Mokuleia beach, Oahu, Hawaii. Fig. 6 shows the site location, bathymetry, and instrument transect profile. The site is open to north swells during the winter months. The open ocean wave conditions are recorded by Buoy 51201 at 200 m water depth. The bathymetry of the Hawaiian Islands is well defined by numerous LiDAR and multi-beam surveys. The slope of the insular shelf on Oahu's north shore is quite gentle from the 200-m depth contour to the shore. The reef, which starts at approximately 20 m water depth, rapidly rises to 10 m and the slope becomes gentler until the reef crest. Six sensors were deployed along a transect across the reef to 20 m depth.

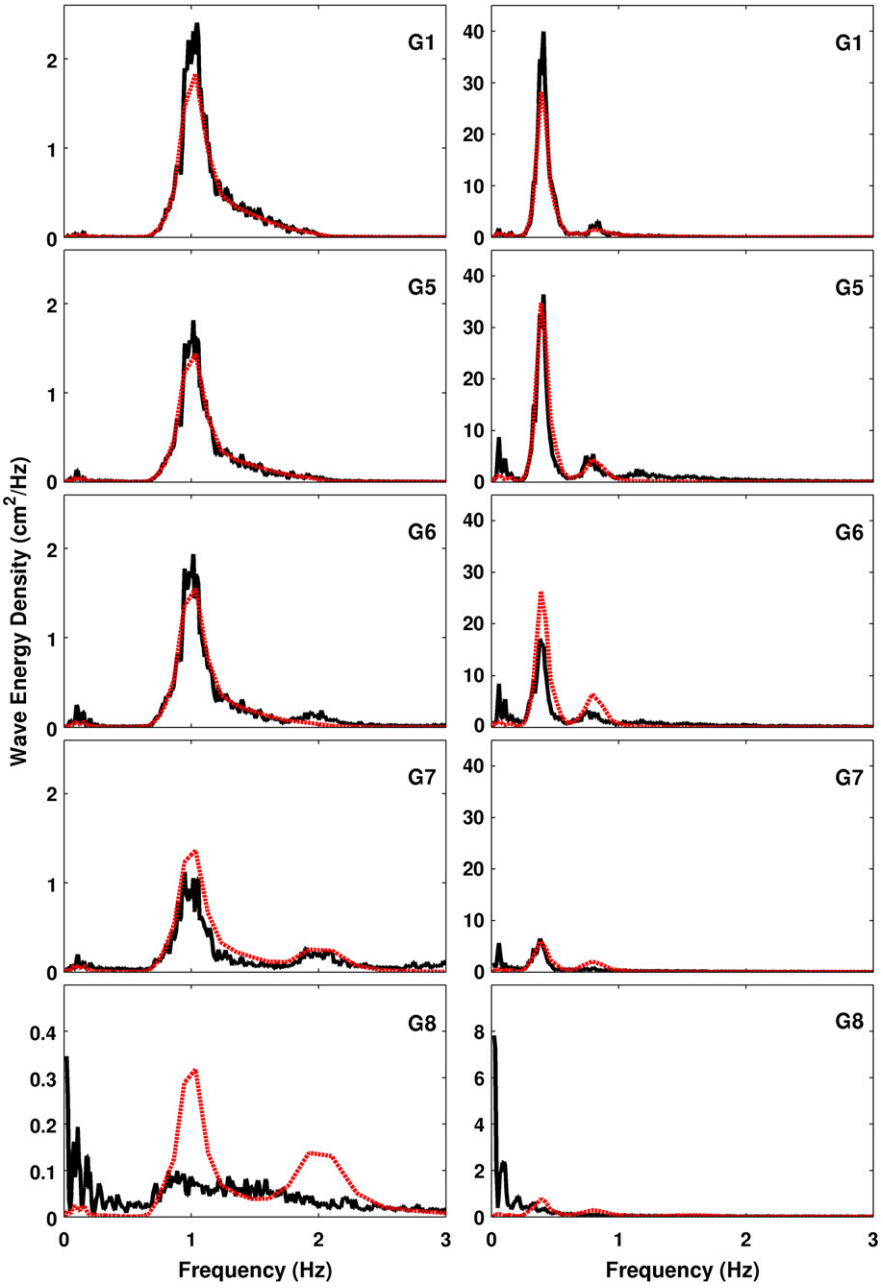

Fig. 5. Comparison of observed and computed wave energy spectra across the reef for Test 44 (low energy) and Test 32 (high energy). Black line: measurements; red line: optimal BJ78 with $\gamma = 0.94$ and $B = 1.09$.

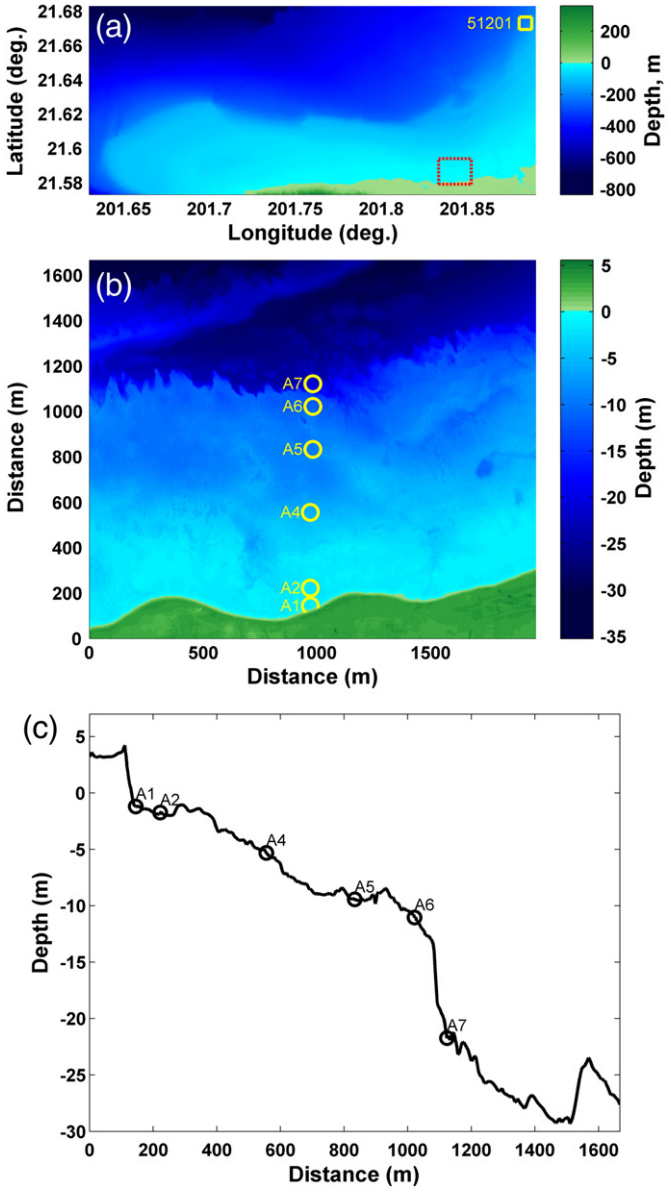

Fig. 6. Site information for the field study. (a) Study site on North Shore, Oahu. (b) Study site at Mokuleia. (c) Instrument transect. Square: buoy 51201; circles: coastal wave sensors.

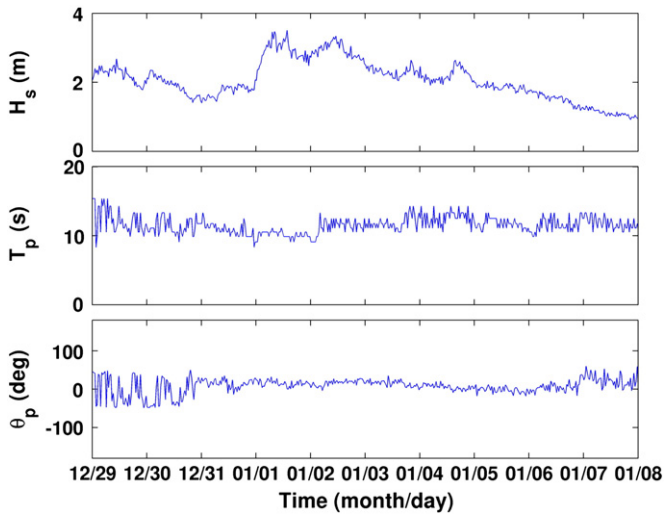

Fig. 7. Recorded offshore wave conditions at buoy 51201 during the field study.

Two of the sensors were located in a shallow lagoon of approximately 1.5 m deep between the reef crest and the shore. Although the profile differs from the laboratory model of Demirbilek et al. (2007), the reef slopes in front of the crest are comparable to produce similar depth-induced breaking processes.

The six sensors provided continuous measurements of the coastal wave conditions from December 28, 2007 to January 8, 2008, during which Buoy 51201 recorded a series of wave events. The recorded significant wave height, peak period, and direction from the National Data Buoy Center are shown in Fig. 7. A north swell event with $H_s = 2$–2.5 m and $T_p = 12$–16 s occurred during the first three days. This is followed by waves with $H_s = 2.5$–3.5 m and $T_p = 10$–12 s due to a system passing through from the north. Strong trade winds were developed on January 3 and 4 augmenting the significant wave height with wind seas. The significant wave height then slowly decreased to about 1 m toward the end of the measurements, while the wave period remained relatively constant at $T_p = 11$–13 s. The site is open to these wave events, which had peak directions varying

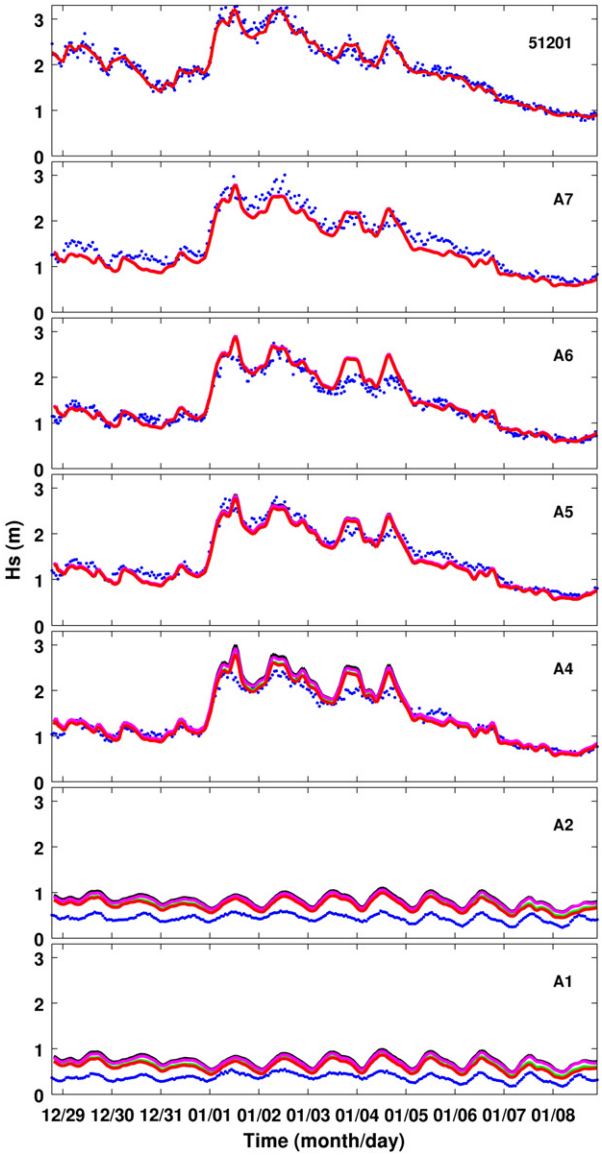

Fig. 8. Comparison of recorded and computed significant wave heights at Mokuleia. Blue dots: observations; black line: JONSWAP; green line: Madsen (1988); magenta line: Collins (1972); and red line: LW05 with $K_w = 0.16$ m.

slightly about the north. The instruments at the site recorded a set of 270 semi-hourly spectra and wave parameters for examination of the model parameterizations. The computation utilizes two levels of nested grids covering the regions shown in Fig. 6a and b. The level-1 grid extends from buoy 51201 to the shore at 1 second resolution, while the level-2 grid covers the instrument transect from 30 m water depth to the shore at 3 m resolution. The spectral data at the Buoy 51201 provides the input conditions to the level-1 grid, which in turn defines the boundary conditions for the level-2 grid. The global tidal model TPXO.6 of Egbert and Erofeeva (2002) defines the water level for the computation. SWAN was run in the non-stationary and Cartesian modes with 36 direction bins and 72 frequency bins from 0.005 to 1 Hz. The optimal BJ78 parameterization for depth-induced wave breaking, the LTA parameterization for the triad interactions, and the wave setup calculation are activated in the level-2 grid.

We first examine the three parameterizations for bottom friction in SWAN as well as Lowe et al. (2005) in their default settings. The significant wave height is estimated from integration of the computed energy density up to 0.2 Hz consistent with the cut-off frequency of the observed spectra. Fig. 8 compares the observed and computed significant wave heights at buoy 51201 and the six sensors at the site. The good agreement between the computed and recorded data at buoy 51201 indicates that the offshore wave conditions are properly input into SWAN. The wave height decreases slightly from the buoy to A7 corresponding to the initial stage of the shoaling process. An average peak period of 12 s during the case study gives a depth parameter of $kd \approx 0.8$ at A7. The wave height should increase shoreward of A7 given the shore-normal, peak wave direction, but the observations and computed results from A7 to A4 show little variation, suggesting a balance between shoaling and dissipation by bottom friction. The model trends to give slightly larger wave heights on the reef slope during the trade wind event on January 3 and 4. Although the north swell is dominant as indicated by the peak wave direction, the sea state is bimodal with a component from the east to northeast associated with the trade winds. While buoy 51201 recorded the full event from an offshore location for model input, the northeast headland of Oahu might have partially shielded the site from the wind waves. This is evident in the reduced signature of the wind waves at the sensors in relation to that at buoy 51201. In contrast, other features recorded at the buoy extend across the reef slope with little attenuation.

The waves break and their height decreases dramatically across the reef crest between A4 and A2. The depth-limited wave heights computed at A2 and A1, which are independent of the offshore conditions, reflect the tide signals quite clearly. The four parameterizations give rise to very similar wave heights across the reef and provide good agreement with the observed data up to A4, but overestimate the significant wave height at A2 and A1 in the shallow lagoon. This is expected for the three default bottom friction parameterizations in SWAN as they were calibrated for sand beds, which are much smoother than the reef at Mokuleia. The LW05 parameterization also over-predicts the significant wave heights at A2 and A1, indicating that the bottom roughness at Mokuleia is likely larger than that at Kaneohe. A closer look at the results suggests that a hydraulic roughness scale of 0.16 m yields acceptable dissipation rates over the reef slope from A7 to A4, but appears to be too small shoreward of A4. Pawlak and MacCready (2002) and Bandet (2009) identified different turbulent flow regimes and dissipation rates over large bedform roughness depending on the wave orbital amplitude and the roughness scale. As stressed by Tolman (1992), most of the errors in the bottom friction parameterization are related to estimation of the appropriate bottom roughness. A single roughness scale thus cannot fully describe the dissipation due to bottom friction at this site.

An aerial photo of the site in Fig. 9 shows an abrupt change of the surface texture and color between A4 and A2 at approximately 5 m depth. The substrate transitions from bare reefs covered by thin layers of light color sand to rough reefs with branching and fossil corals (Jaramillo and Pawlak, 2011). This corresponds to an increase of the bottom roughness from the reef slope to the crest and the inner region.

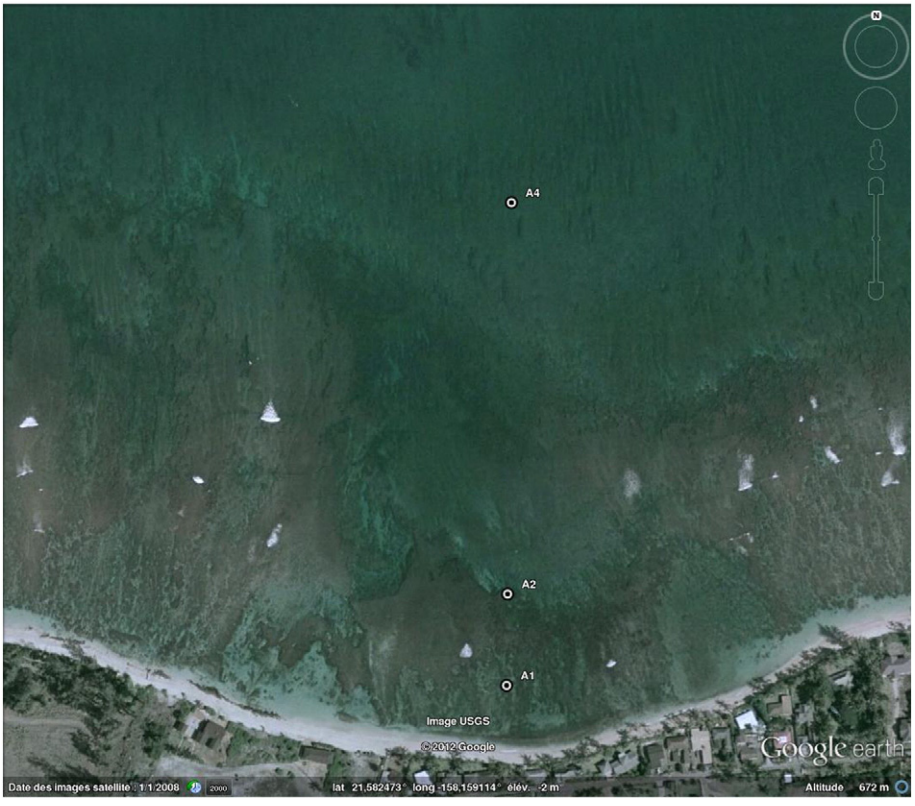

Fig. 9. Aerial image of the reef and sensor locations at Mokuleia from Google Earth.

Despite being qualitative, the observed bottom roughness suggests that the model results might be improved by using a higher roughness scale for the nearshore region. Since our knowledge on the spatial variability is limited, we assume an abrupt transition at the 5-m contour from $K_w = 0.16$ m to a higher value. Through a sensitivity analysis, we obtained $K_w = 0.5$ m in the nearshore region to match the recorded data at A2 and A1. Fig. 10 compares the recorded and computed significant wave heights with and without the abrupt increase of the nearshore roughness scale. The energy dissipation from A4 to A2 is from a combination of wave breaking and bottom friction, but as the offshore significant wave height decreases to less than 1 m toward the end the case study, bottom friction becomes the dominant process. The use of $K_w = 0.5$ m appears to work well over the range of significant wave heights during the event, rendering support for both the wave-breaking and bottom-friction parameterizations. The use of the large K_w here is not to offset underestimations of wave breaking dissipation as verified toward the end of the case study when wave breaking becomes unimportant and bottom friction dominates the dissipation from A4 to A2. In addition, the selected roughness scale correctly accounts for the dissipation from A2 to A1 with no wave breaking involved. This bottom roughness scale is higher than that at Kaneohe, but corroborates visual observations made at the site and measurements on the south shore of Oahu by Nunes and Pawlak (2008).

The comparison with the flume experiment in Section 3 has already shown that an accurate description of wave height attenuation across the reef is important for estimation of the wave setup. We thus utilize the composite roughness scale of $K_w = 0.16$ and 0.5 m in the LW05 parameterization to examine the wave setup in natural reef environments. Fig. 11 compares the computed and recorded wave setup at A1 for the entire case study and along the instrument transect during the rise, peak, and decay of the swell event from December 31, 2009 to January 5, 2008. The observed wave setup is estimated from the surface elevation time series using the global tidal model TPXO.6 of Egbert and Erofeeva (2002). This might introduce errors into the deduced data as the global tidal model does not resolve island-scale processes. Nevertheless, the model reproduces the observed wave setup reasonably well especially for the energetic events in which the signal to noise level is high. The swell reaches 1.95 m significant wave height at buoy 51201 on December 31. The waves break at the reef crest causing an increase of the mean water level in the lagoon. The peak arrives in the morning of January 2 with an offshore wave height of 3 m and produces breaking waves on the upper reef slope resulting in a wider surf zone. The setup retreats

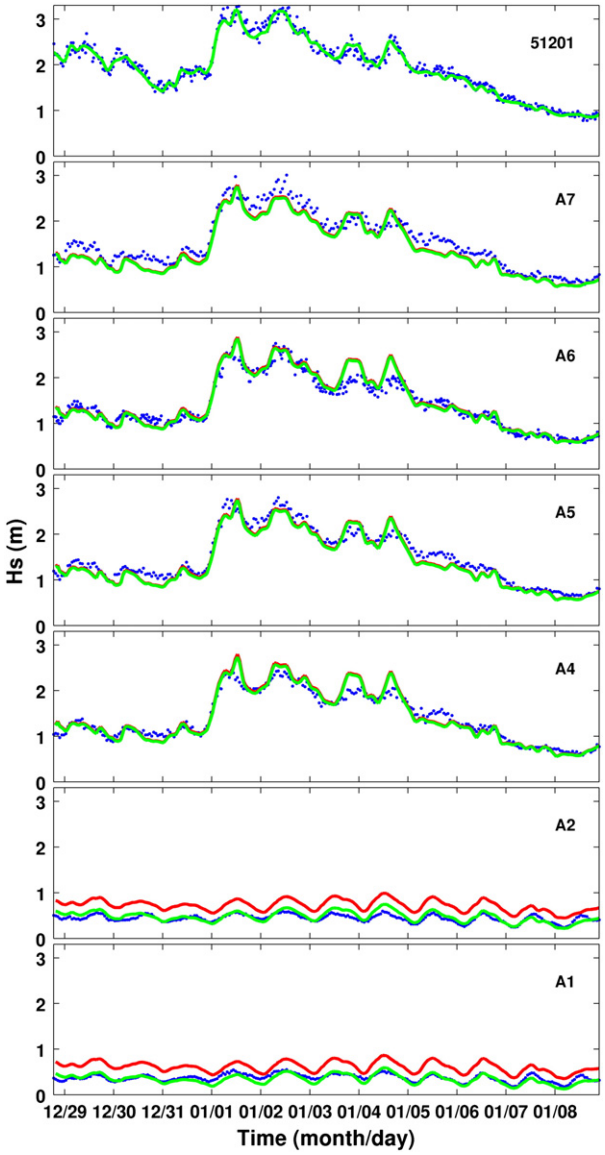

Fig. 10. Comparison of recorded and computed significant wave heights at Mokuleia. Blue dots: observations; red line: LW05 with $K_w = 0.16$ m; green line: LW05 with $K_w = 0.16$ and 0.5 m.

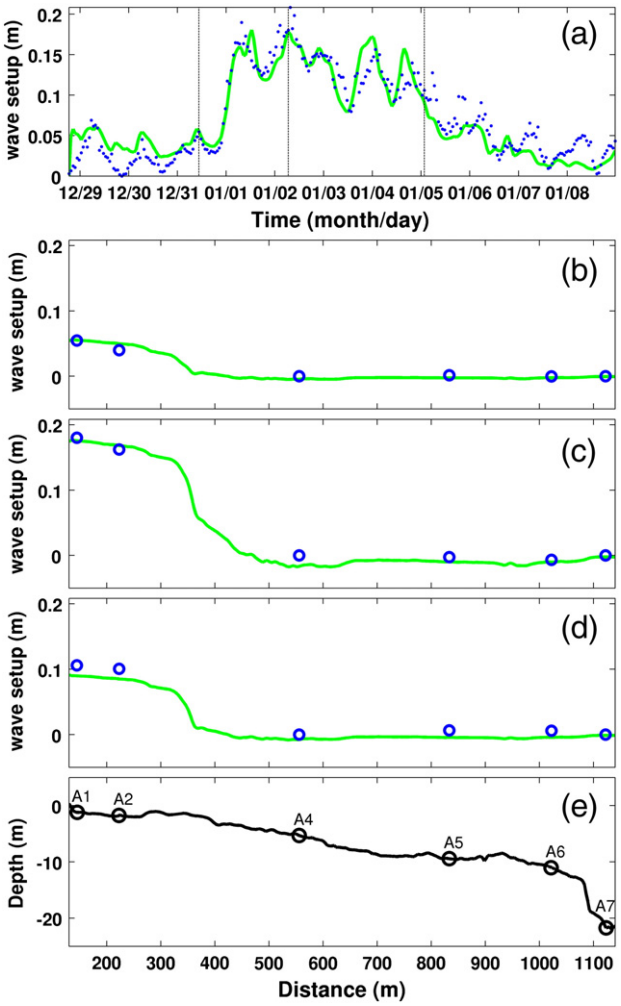

Fig. 11. Comparison of recorded and computed wave setup at Mokuleia. (a) Wave setup at A1 during the entire case study. (b) Wave setup on 31/12/2007 10:34 am. (c) Wave setup on 1/2/2008 6:34 am. (d) Wave setup on 1/5/2008 1:34 am. (e) Reef profile along the instrument transect. Blue dots and circles: recorded data; green line: LW05 with $K_w = 0.16$ and 0.5 m.

back to the lagoon during the decay of the swell when the offshore significant wave height reduces to 1.95 m in the early morning of January 5. The model captures the slight increase of wave setup from A2 to A1 in the lagoon because of the correct depiction of energy dissipation due to bottom roughness. The rapid water-level build-up over the reef slope and a gradual increase in the lagoon are unique to tropical coastal environments.

The transformation of the observed spectrum across the reef provides insights into the triad interactions and the ability of the LTA parameterization in describing these processes in natural reef environments. We selected two distinct records for this purpose and present the results in Fig. 12. The first record at 2:34 pm on January 1 corresponds to the peak of the swell event and the second one represents less energetic conditions toward the end of the case study on January 8, 6:34 am. Both events reveal similar trends albeit the large difference in energy level. The model reasonably reproduces the observed spectra from buoy 51201 to A4, while discrepancies between the observed and computed spectra are evident at A2 and A1 in the back-reef region. The broadening of the spectra to low frequencies is not reproduced by the model. The LTA parameterization transfers energy to the superharmonics during shoaling and breaking and accounts for some of the high-frequency energy in the lagoon. Even though the energy levels are much lower at A1 and A2, the recorded data clearly shows a dominant sub-harmonic component that is not captured by SWAN due to the lack of appropriate parameterization. Infragravity waves are of primary importance in nearshore processes, as they drive currents and transport sediment, and need special attention in spectral wave modeling.

5. Conclusions and recommendations

Spectral wave models rely on parameterizations of nonlinear coastal processes such as wave breaking, bottom friction, and wave interaction on gentle-sloping beaches. Recorded data from a laboratory experiment and a field study allows examination of these parameterizations for fringing reef environments. The comparison of model data from SWAN with the laboratory data demonstrates that the default wave-breaking parameterizations are not able to capture the sharp build-up and decay

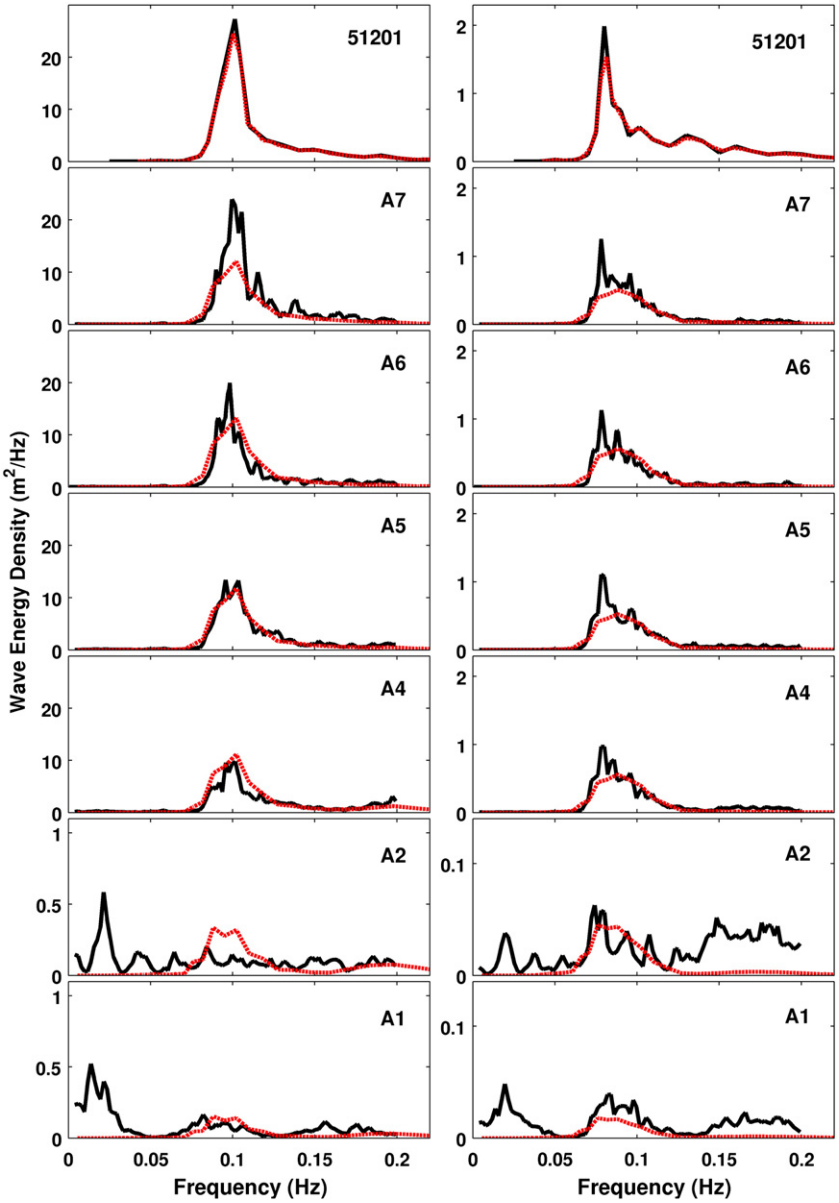

Fig. 12. Comparison of recorded and computed wave spectra for high and low-energy waves at Mokuleia. Black line: observed spectra; red dotted line: computed spectra using LW05 with $K_w = 0.16$ and 0.5 m.

of the wave height associated with the energetic breaking process at the reef crest. An ad hoc calibration of the parameterization of Battjes and Janssen (1978) improves the overall model performance. The NRMSE decreases by 39% with the use of the optimal parameters $B = 1.09$ and $\gamma = 0.94$. The improved description of wave attenuation provides a better estimate of the wave setup on the reef flat.

The field data covers two north swell events with breaking and non-breaking wave conditions for examination of bottom-friction parameterizations. The results highlight the importance of bottom roughness in wave transformation over fringing reefs. Published parameterizations for bottom friction can adequately describe the dissipation over most of the reef slope, but underestimate the effects over the nearshore reef, where the surface is observed to be highly irregular. Calibration of the parameterization of Lowe et al. (2005) gives a roughness scale of 0.5 m in the nearshore region in comparison to the adopted value of 0.16 m over the reef slope. This works well with the optimal wave-breaking parameterization of Battjes and Janssen (1978) to reproduce the wave height and setup across the fringing reef for a full range of wave conditions and to provide a framework for calibration of spectral wave models using data from other PILOT project sites.

Both the laboratory and field data shows transfer of energy from the spectral peak to the sub and super-harmonics as the waves propagate across the reef. The LTA triad parameterization of Eldeberky (1996) describes the transfer of energy to the super-harmonics associated with increasing wave nonlinearity during the shoaling phase. However, the transfer of energy to the infragravity band is, by construction of SWAN, not taken into account. This leads to omission of an important wave component in the inner reef region that might for instance produces seiches and other coastal hazards. With recent advances in fully nonlinear, triad interaction models, future research should be directed toward a complete parameterization of the triad wave–wave interactions for spectral wave modeling.

Acknowledgment

The Department of Energy supported this research through Grant No. DE-FG36-08GO18180 via the National Marine Renewable Energy Center at the University of Hawaii. The authors would like to thank Dr. Okey Nwogu for the laboratory data, Dr. Jane Smith for the field data from the PILOT project, Prof. Mark Merrifield, Prof. Janet Becker, and Mr. Justin Stopa for their assistance with this study, and the two anonymous referees for their comments and suggestions on the paper. SOEST Contribution No. 8543.

References

Abelson, A., Miloh, T., Loya, Y., 1993. Flow patterns induced by substrata and body morphologies of benthic organisms, and their roles in determining availability of food particles. Limnology and Oceanography 38 (6), 1116–1124.

Apotsos, A., Raubenheimer, B., Elgar, S., Guza, T.G., 2008. Testing and calibrating parametric wave transformation models on natural beaches. Coastal Engineering 55, 224–235.

Arcilla, A.S., Roelvink, J.A., O'Connor, B.A., Reniers, A.J.H.M., Jimenez, J.A., 1994. The Delta Flume '93 experiment. Proc. Coastal Dynamics Conf. ASCE, Barcelona, Spain.

Ardhuin, F., Rogers, E., Babanin, A., Filipot, J.-F., Magne, R., Roland, A., van der Westhuysen, A., Queffeulou, P., Lefevre, J.-M., Aouf, L., Collard, F., 2010. Semi-empirical dissipation source function for wind-wave models: part 1, definition, calibration and validation at global scales. Journal of Physical Oceanography 40 (9), 1917–1941.

Bandet, M., 2009. Dynamics of wave-induced boundary layer over very rough boundaries: field observations over a stretch of coral reef. Ph.D. Dissertation, University of Hawaii, Honolulu.

Battjes, J.A., Janssen, J.P.F.M., 1978. Energy loss and set-up due to breaking of random waves. Proceedings of the 16th International Conference on Coastal Engineering. ASCE, pp. 569–587.

Battjes, J., Stive, M., 1985. Calibration and verification of a dissipation model for random breaking waves. Journal of Geophysical Research 90 (C5), 9159–9167.

Battjes, J.A., Beji, S., 1992. Breaking waves propagating over a shoal. Proc. 23rd Int. Conf. Coastal Eng., Venice, Italy, pp. 42–50. S.

Bertotti, L., Cavaleri, L., 1994. Accuracy of wind and wave evaluation in coastal regions. Proc. 24th Int. Conf. Coastal Engineering, Kobe. ASCE, New York, pp. 57–67.

Booij, N., Ris, R.C., Holthuijsen, L.H., 1999. A third-generation wave model for coastal regions. 1. model description and validation. Journal of Geophysical Research 104 (C4), 7649–7666 (Apr.).

Cheung, K.F., Tang, L., Donnelly, J.P., Scileppi, E., Liu, K.-B., Mao, X.Z., Houston, S.H., Murnane, R.J., 2007. Numerical modeling and field evidence of coastal overwash in southern New England from Hurricane Bob and implications for paleotempestology. Journal of Geophysical Research 112 (3), F03024. http://dx.doi.org/10.1029/2006JF000612.

Collins, J.I., 1972. Prediction of shallow-water spectra. Journal of Geophysical Research 77 (15), 2693–2707 May.

Demirbilek, Z., Nwogu, O.G., Ward, D.L., 2007. Laboratory study of wind effect on runup over fringing reefs, report 1: data report. Tech. Rep., US Army Corps of Engineers, Vicksburg, Mississippi.

Dietrich, J.C., Zijlema, M., Westerink, J.J., Holthuijsen, L.H., Dawson, C., Luettich, R.A., Jensen, R., Smith, J.M., Stelling, G.S., Stone, G.W., 2010. Modeling hurricane waves and storm surge using integrally-coupled, scalable computations. Coastal Engineering 58 (1), 45–65.

Dingemans, M.W., Radder, A.C., Vriend, H.J., 1987. Computation of the driving forces of wave-induced currents. Coastal Eng. 11, 539–563.

Egbert, G.D., Erofeeva, S.Y., 2002. Efficient inverse modeling of barotropic ocean tides. Journal of Atmospheric and Oceanic Technology 19 (2), 183–204.

Eldeberky, Y., 1996. Nonlinear transformation of wave spectra in the nearshore zone. Ph.D. thesis, Delft University of Technology, The Netherlands.

Eldeberky, Y., Battjes, J., 1996. Spectral modeling of wave breaking: application to Boussinesq equations. Journal of Geophysical Research 101 (C1), 1253–1264.

Filipot, J.-F., Ardhuin, F., Babanin, A.V., 2010. A unified deep-to-shallow water wave-breaking probability parameterization. Journal of Geophysical Research 115 (C04022). http://dx.doi.org/10.1029/2009JC005448.

Filipot, J.-F., Ardhuin, F., in press. A unified spectral parameterization for wave breaking: from the deep ocean to the surf zone. J. Geophys. Res.

Gelci, R., Cazalé, H., Vassal, J., 1957. Prévision de la houle. La méthode des densités spectro-angulaires. Bulletin d'information du Comité d'Océanographie et d'Etude des Côtes 9, 416–435.

Goda, Y., 1975. Irregular wave deformation in the surf zone. Coastal Engineering Japan 18, 13–26.

Hasselmann, K., Barnett, T.P., Bouws, E., Carlson, H., Cartwright, D.E., Enke, K., Ewing, J.A., Gienapp, H., Hasselmann, D.E., Kruseman, P., Meerburg, A., Müller, P., Olbers, D.J., Richter, K., Sell, W., Walden, H., 1973. Measurements of wind-wave growth and swell decay during the Joint North Sea Wave Project. Deutsche Hydrographische Zeitschrift 8 (12), 1–95 (Suppl. A).

Hasselmann, K., Collins, J.I., 1968. Spectral dissipation of finite depth gravity waves due to turbulent bottom friction. Journal of Marine Research 26, 1–12.

Holthuijsen, L.H., 2007. Waves in Oceanic and Coastal Waters. Cambridge University Press, Cambridge, England. 387pp.

Jonsson, I.G., 1967. Wave boundary layers and friction factors. Proceedings of the 10th International Conference on Coastal Engineering. ASCE, Tokyo, Japan, pp. 127–148.

Jaramillo, S., Pawlak, G., 2011. AUV-based bed roughness mapping over a tropical reef. Coral Reefs 30 (SI1), 11–23.

Komen, G.J., Cavaleri, L., Donelan, M., Hasselmann, K., Hasselmann, S., Janssen, P.A.E.M., 1994. Dynamics and Modelling of Ocean Waves. Cambridge Univ. Press, New York. 532pp.

Longuet-Higgins, M.S., 1974. On the mass, momentum, energy and circulation of a solitary wave. Proc. R. Soc. Lond. A 337, 1–13.

Lowe, R.J., Falter, J.L., Bandet, M.D., Pawlak, G., Atkinson, M.J., Monismith, S.G., Koseff, J.R., 2005. Spectral wave dissipation over a barrier reef. Journal of Geophysical Research 110 (C04001). http://dx.doi.org/10.1029/2004JC002711.

Lugo-Fernández, A., Roberts, H.H., Suhayda, J.N., 1998. Wave transformations across a Caribbean fringing-barrier coral reef. Continental Shelf Research 18 (10), 1099–1124.

Madsen, O.S., 1994. Spectral wave-current bottom boundary layer flows. Proceedings of the 24th International Conference on Coastal Engineering. ASCE, pp. 384–397.

Madsen, P.A., Sørensen, O.R., 1993. Bound waves and triad interactions in shallow water. Ocean Eng. 20 (4), 359–388.

Massel, S.R., Gourlay, M.R., 2000. On the modeling of wave breaking and set-up on coral reefs. Coastal Engineering 39 (1), 1–27.

Mirfenderesk, H., Young, I.R., 2003. Direct measurements of the bottom friction factor beneath surface gravity waves. Applied Ocean research 25 (5), 269–287.

Nelson, R., 1987. Design wave heights on very mild slopes: an experimental study. Civil Engineering Transactions 29, 157–161.

Nelson, R., 1994. Depth limited wave heights in very flat regions. Coastal Engineering 23 (1–2), 43–59.

Nielsen, P., 1992. Coastal Bottom Boundary Layers and Sediment Transport. World Scientific Publishing.

Nunes, V., Pawlak, G., 2008. Observations of bed roughness of a coral reef. Journal of Coastal Research 24 (2B), 39–50.

Madsen, O., 1988. Spectral wave attenuation by bottom friction: theory. 21st International Conference on Ocean Engineering. ASCE, pp. 492–504.

Pawlak, G., MacCready, P., 2002. Oscillatory flow across an irregular boundary. Journal of Geophysical Research 107 (C53036). http://dx.doi.org/10.1029/2000JC000596.

Péquignet, A.-C., Becker, J., Merrifield, M., Boc, S., 2011. The dissipation of wind wave energy across a fringing reef at Ipan, Guam. Coral Reefs 30 (SI1), 71–82.

Raubenheimer, B., Guza, R.T., Elgar, S., 1996. Wave transformation across the inner surf zone. Journal of Geophysical Research 101 (C10), 2589–2597.

Ris, R.C., Booij, N., Holthuijsen, L.H., 1999. A third-generation wave model for coastal regions. 2. Verification. Journal of Geophysical Research 104 (C4), 7667–7681.

Roeber, V., Cheung, K.F., Kobayashi, M., 2010a. Shock-capturing Boussinesq-type model for nearshore wave processes. Coastal Engineering 57 (4), 407–423.

Roeber, V., Yamazaki, Y., Cheung, K.F., 2010b. Resonance and impact of the 2009 Samoa tsunami around Tutuila, American Samoa. Geophysical Research Letters 37 (21), L21604. http://dx.doi.org/10.1029/2010GL044419.
Ruessink, B.G., Walstra, D.J.R., Southgate, H.N., 2003. Calibration and verification of a parametric wave model on barred beaches. Coastal Engineering 48 (3), 139–149.
Shemdin, P., Hasselmann, K., Hsiao, S.V., Herterich, K., 1978. Non-linear and linear bottom interaction effects in shallow water. In: Favre, A., Hasselmann, K. (Eds.), Turbulent Fluxes through the Sea Surface, Wave Dynamics and Prediction. Plenum, New York, pp. 347–372.
Sheremet, A., Kaihatu, J.M., Su, S.-F., Smith, E.R., Smith, J.M., 2011. Modeling of nonlinear wave propagation over fringing reefs. Coastal Engineering 58 (12), 1125–1137.
Thornton, E.B., Guza, R.T., 1983. Transformation of wave height distribution. Journal of Geophysical Research 88 (C10), 5925–5938.
Tolman, H.L., 1992. An evaluation of expressions for wave energy dissipation due to bottom friction in the presence of currents. Coastal Engineering 16 (2), 165–179.
Tolman, H.L., 2008. A mosaic approach to wind wave modeling. Ocean Modelling 25 (1–2), 35–47.
van der Westhuysen, A.J., 2010. Modeling of depth-induced breaking under finite depth wave growth conditions. Journal of Geophysical Research 115 (C011008). http://dx.doi.org/10.1029/2009JC005433.
Vetter, O., Becker, J.M., Merrifield, M.A., Péquignet, A.-C., Aucan, J., Boc, S.J., Pollock, C.E., 2010. Wave setup over a Pacific island fringing reef. Journal of Geophysical Research 115 (C12066). http://dx.doi.org/10.1029/2010JC006455.
Vink, A., 2001. Transformation of wave spectra across the surf zone. Master's thesis, Delft University of Technology, The Netherlands.
Zijlema, M., 2010. Computation of wind-wave spectra in coastal waters with SWAN on unstructured grids. Coastal Engineering 57 (3), 267–277.

Further reading

Ardhuin, F., Herbers, T.H.C., O'Reilly, W.C., 2002. A hybrid Eulerian-Lagrangian model for spectral wave evolution with application to bottom friction on the continental shelf. J. Phys. Oceanogr. 31, 1498–1516.
Longuet-Higgins, M.S., Stewart, R.W., 1962. Radiation stresses and mass transport in surface gravity waves with application to 'surf beats'. Journal of Fluid Mechanics 13, 481–504.
Nelson, R., 1997. Height limits in top down and bottom up wave environments. Coastal Engineering 32 (2–3), 247–254.
Tolman, H.L., 1994. Wind waves and moveable-bed bottom friction. Journal of Physical Oceanography 24 (5), 994–1009.